Journal of Alloys and Compounds 509 (2011) 9098–9104

Contents lists available at ScienceDirect

Journal of Alloys and Compounds

journal homepage: www.elsevier.com/locate/jallcom

Magnetic and luminescent properties of $Fe/Fe_3O_4@Y_2O_3$:Eu nanocomposites

Qin Wang[a,b], Xuwei Yang[a], Lianxiang Yu[a], Hua Yang[a,*]

[a] College of Chemistry, Jilin University, Changchun 130012, China
[b] College of Chemistry and Chemical Engineering, Inner Mongolia University, Hohhot, China

ARTICLE INFO

Article history:
Received 30 May 2011
Received in revised form 13 June 2011
Accepted 14 June 2011
Available online 6 July 2011

Keywords:
Magnetic
Luminescence
Fe/Fe_3O_4
Y_2O_3:Eu
Nanocomposites

ABSTRACT

Multifunctional nanocomposites with Fe/Fe_3O_4 nanoparticles as the core and europium-doped yttrium oxide (Y_2O_3:Eu) as the shell ($Fe/Fe_3O_4@Y_2O_3$:Eu) have been obtained successfully employing a solvothermal method. The nanocomposites showed both ferrimagnetic behavior and unique europium fluorescence properties with high emission intensity. The spectra changes induced by the UV light irradiation and the magnetic field have been systematically studied and compared in detail. The relationship between fluorescence and magnetic properties of the multifunctional nanocomposites has been investigated in our manuscript. These multifunctional nanocomposites could be used in a number of biomedical applications, such as drug targeting, cell separation and bioimaging.

1. Introduction

Multifunctional nanocomposites have attracted considerable attention in recent years because of their desirable properties and relevant applications. For instance, nanocomposites with both magnetic and fluorescent properties can be used in a wide range of applications in biological systems, such as targeted drug, diagnostic, therapeutics and bioimaging [1–5]. They can be controlled by an external magnetic field; they can also serve as luminescent phosphors.

Most of the magnetic and fluorescent nanocomposites are core–shell structures with the magnetic particles as the core and the fluorescent phosphor as the shell. To the best of our knowledge, there are a few reports on the synthesis of multifunctional nanocomposites consisting of a magnetic core with a phosphor shell [6–15]. However, the formation of the core–shell structured nanocomposites in these papers are all conventionally followed by an encapsulation process, where the magnetic cores are encapsulated by the silica shell using a sol–gel technique. After been encapsulated by the silica shell, the saturation magnetization of the multifunctional nanocomposites decreased dramatically. And the size of the multifunctional nanocomposites increased. At present, there are few reports on the direct combination of magnetic particles with lanthanide nano-phosphors. Lu et al. deposited a shell of up-converting phosphor on an iron oxide core [16]. Kennedy et al. synthesized multifunctional $Fe_3O_4@Y_2O_3$:Eu nanocomposites by a facile homogenous precipitation method [1]. However, the relationship between the magnetic and fluorescent properties is rarely discussed, including the changes of the magnetic and fluorescent properties under the UV-light irradiation and the magnetic field effects.

Here we report the synthesis and properties of magnetic/fluorescent nanocomposites with Fe/Fe_3O_4 nanoparticles as the core and the Y_2O_3:Eu as the shell. Then we discussed the relationship between the magnetic and fluorescent properties. The changes of the magnetic and fluorescent properties under the UV-light irradiation and the magnetic field effects are investigated in detail. Finally, we explained the changes of the magnetic and fluorescent properties under the UV-light irradiation and the magnetic field effects.

2. Experimental

2.1. Reagents and materials

All chemicals were of analytical grade and were used as received without further purification. Deionized water was used. Ferrous chloride tetrahydrate ($FeCl_2{\cdot}4H_2O$), ethanol absolute, tetramethyl ammonium hydroxide (TAH) ($N(CH_3)_4OH$), n-hexane (C_6H_{14}), sodium oleate ($C_{18}H_{33}NaO_2$), Ln_2O_3 (Y_2O_3, Eu_2O_3 purity >99.99%) were all purchased from the Beijing Chemical Reagent Company.

2.2. Synthesis of Fe/Fe_3O_4 nanoparticles

Stoichiometric molar ratios of starting materials were dissolved in distilled water, and corresponding chloride solutions were obtained. In a typical synthesis, 5 mmol of $FeCl_2{\cdot}4H_2O$ was dissolved in 35 ml of mixture solution (15 ml ethanol absolute, 15 ml n-hexane and 5 ml H_2O) under N_2 atmosphere with vigorous stirring. After 30 min, 3.5 g sodium oleate was added into the mixed solution. Then 10 ml of

* Corresponding author.
E-mail address: huayang86@sina.com (H. Yang).

0925-8388/$ – see front matter.
doi:10.1016/j.jallcom.2011.06.058

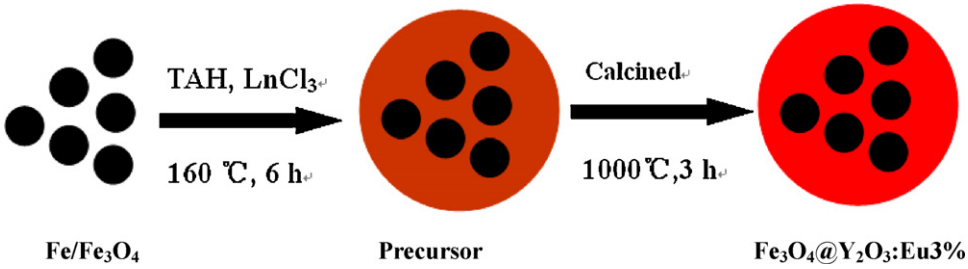

Scheme 1. Synthetic scheme for the synthesis and surface modification of multifunctional Fe_3O_4@Y_2O_3:Eu3% nanocomposites.

TAH was added dropwise. The mixture was stirred continually for another 30 min and then transferred into a 50 ml Teflon lined stainless steel autoclave, sealed and maintained at 180 °C for 3 h. After completion of the reaction, the black solid products were collected by magnetic separation and washed several times with water and ethanol. The final products were dried in a vacuum oven at 40 °C for 6 h.

2.3. Synthesis of Y_2O_3:Eu3% microspheres

In a typical synthesis, appropriate amounts of high purity Y_2O_3 and Eu_2O_3 (C 99.999%) were dissolved in concentrated HNO_3 (65%) to form nitrate solutions. 2.5 g CH_3COONa and 37 ml mixing solution of EG and water (volume ratio for EG:H_2O = 35:2) were added to the nitrate solutions. Then additional of TAH was slowly added to the above solution and adjusted to a designated pH of 12. The mixture was then transferred into a 50 ml Teflon lined stainless steel autoclave, sealed and maintained at 160 °C for 6 h. The resulting suspension was allowed to cool to room temperature naturally. After centrifugation, washed with absolute ethanol and distilled water for several times, the white precipitate was obtained. Finally, the white precipitate was dried in vacuum at 40 °C for 12 h, and calcined at 1000 °C for 3 h.

2.4. Synthesis of multifunctional Fe/Fe_3O_4 @Y_2O_3:Eu3% nanocomposites

Y_2O_3:Eu phosphor was coated on the magnetic Fe/Fe_3O_4 nanoparticles by using a solvothermal method (Scheme 1). In a typical synthesis, 15 mg of Fe/Fe_3O_4 nanoparticles were dispersed in 10 ml ethanol absolute containing 20 mM $Ln(NO_3)_3$(Ln = Y, Eu; Eu^{3+} doping concentration was 3%). 2.5 g CH_3COONa and 37 ml mixing solution of EG and water (volume ratio for EG:H_2O = 35:2) were added to the nitrate solutions. The mixture was sonicated for 30 min and the pH was adjusted to 12 by TAH. Then the mixture was transferred into a 50 ml Teflon lined stainless steel autoclave, sealed and maintained at 160 °C for 6 h. After completion of the reaction, the products were collected and washed several times with water and ethanol. The final products were dried in a vacuum oven at 40 °C for 6 h. Finally, the precursor particles were clacinated at 1000 °C for 3 h for complete conversion to the oxide. The resulting multifunctional products were magnetic-fluorescent Fe/Fe_3O_4 @Y_2O_3:Eu3% nanocomposites.

2.5. Characterization of Fe/Fe_3O_4 @Y_2O_3:Eu3% nanocomposites

X-ray diffraction (XRD) patterns were performed on a Tokyo X-ray diffractometer with Cu Kα radiation (λ = 0.15405 nm). The morphologies and structures of the as synthesized products were observed with a scanning electron microscopy (SEM) (Philips XL30FEG) and a transmission electron microscope (TEM) (JEOL-2010, 200 kV). To prepare the samples for SEM studies, dried samples were dispersed in ethanol, and the resultant suspensions were sonicated for 1–2 h. Then placed a drop of the composite particle suspension on a piece of microglass slide attached to a metal grid, and dried it gradually at room temperature. The sample was then sputter coated with gold to assess the particle size and shape. All the samples for the TEM characterization were prepared by directly transferring the suspended products to the standard copper grid coated with an amorphous carbon film. For this measurement, the samples were obtained by diluting the dispersed solution with ethanol and then placing a drop of the diluted solution onto a covered copper grid and evaporated in air at room temperature. Before the samples were withdrawn, the composites dispersing in the ethanol solutions were sonicated for 30 min to obtain the better particles dispersion on the copper grid. Magnetic measurements were carried out at room temperature using a Superconducting quantum interference device (SQUID) magnetometer with a maximum magnetic field of 1 T.

3. Results and discussion

In order to investigate the structure and composition of the nanocomposites, XRD was employed to analyze the samples. Fig. 1 shows the XRD pattern of multifunctional Fe/Fe_3O_4@ Y_2O_3:Eu3% nanocomposites after clacination at 1000 °C for 3 h. The magnetic-fluorescent of Fe/Fe_3O_4@Y_2O_3:Eu3% nanocomposites exhibit the characteristic diffraction peaks of Fe_3O_4 (marked with ●) with reverse spinel structure and additional peaks that coincide with the peaks of cubic structure of Y_2O_3 (marked with □). No other impurity peaks were detected. In addition, the peaks of the Fe in multifunctional nanocomposites are not reflected in Fig. 1 because of the relatively lower molar concentration.

SEM and TEM were used to characterize the morphology and crystal structure of the products. SEM images of pure Y_2O_3:Eu3% microspheres and Fe/Fe_3O_4@Y_2O_3:Eu3% nanocomposites with different magnifications are shown in Fig. 2, respectively. From the SEM images of the pure Y_2O_3:Eu3% microspheres (Fig. 2a and b), we can observe that the samples consist of a large quantity of submicrometer scale particles with average diameter of about 2 μm. The SEM images indicate that these microparticles are spherical in shape and uniform in size. The diameter of the microspheres is mainly centered at 2 μm. These particles are non-aggregated with narrow size distribution. The SEM image also reveals the surface configuration of the microspheres. The rough surface of the spherical microsphere implies that these microspheres may be comprised of smaller subunits.

The structural and morphological features of the samples were also investigated by TEM, as shown in Fig. 3. Fig. 3a and 3b shows TEM and selected area electron diffraction (SAED) patterns of the Fe/Fe_3O_4 nanoparticles. As shown in Fig. 3a, the solvothermal treatment based on the ferrous ions disproportionation methods

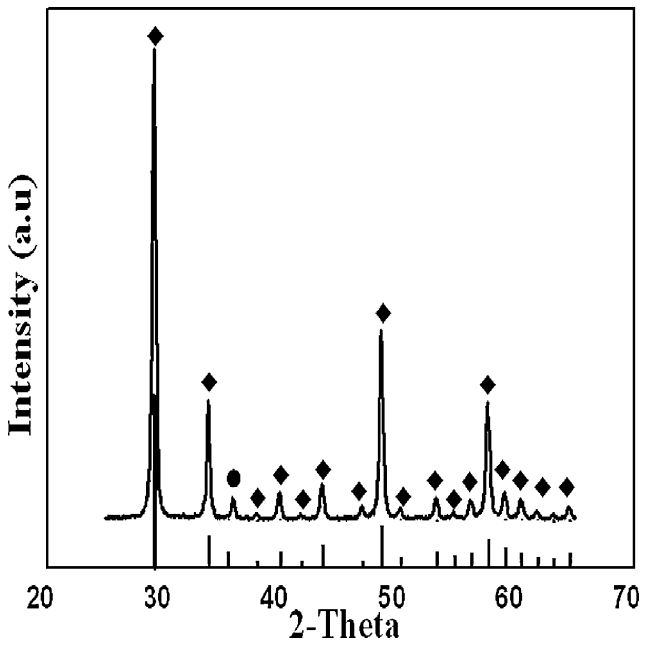

Fig. 1. XRD pattern of magnetic-fluorescent Fe_3O_4@Y_2O_3:Eu3% nanocomposites. The diffraction peaks marked with ● are indexed to Fe_3O_4, and the peaks marked with ♦ are indexed to Y_2O_3:Eu.

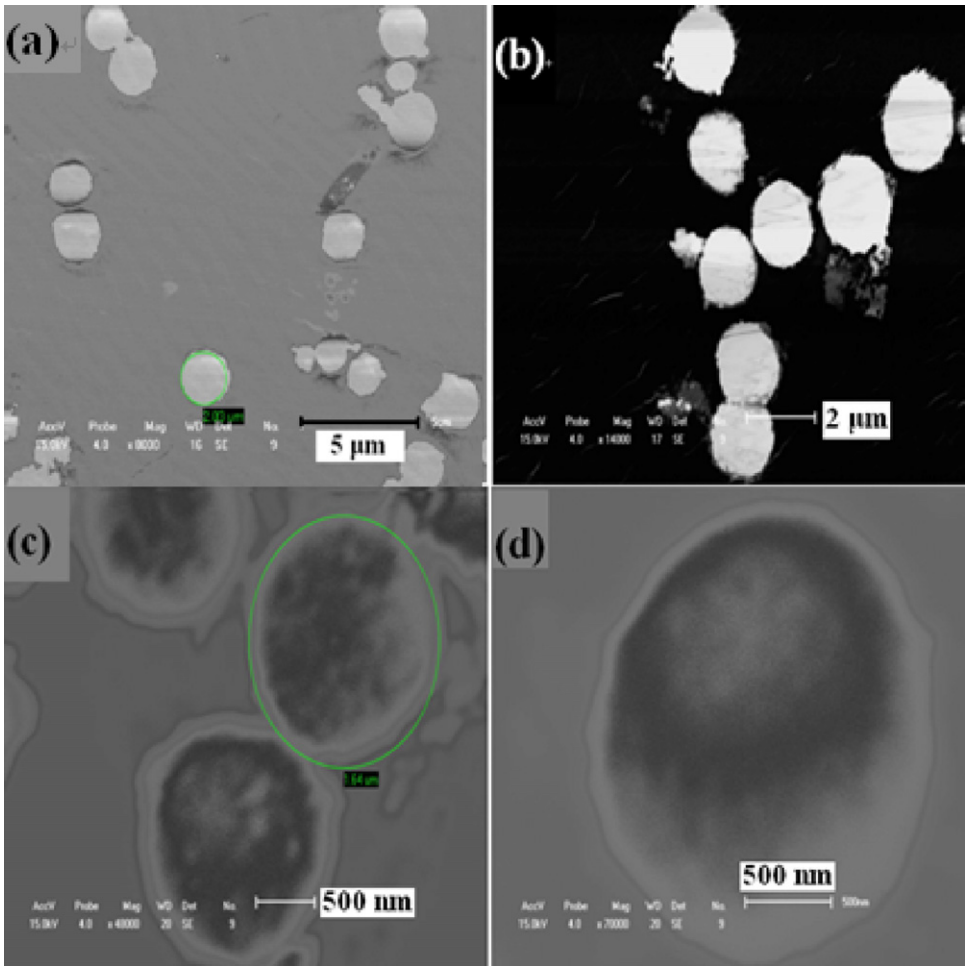

Fig. 2. Low magnification SEM images of (a) and (b) Y_2O_3:Eu3%, (c) and (d) magnetic-fluorescent Fe_3O_4@Y_2O_3:Eu3% nanocomposites.

resulted in the spherical nanoparticles with average diameter of 20 nm. The selected area electronic diffraction (SAED) pattern of the sample is consistent with the high crystallinity, and the diffraction spots could be indexed as the spinel phase of the magnetite. Fig. 3c and d shows that the multifunctional Fe/Fe_3O_4@Y_2O_3:Eu3% nanocomposites still keep the morphological properties of pure Fe/Fe_3O_4 nanoparticles except for a larger particle size, which may be caused by the coating of Y_2O_3:Eu3% on the surface of the magnetic nanoparticles.

Fig. 4 shows the luminescent excitation and emission spectra of the Y_2O_3:Eu3% and Fe/Fe_3O_4@Y_2O_3:Eu3% nanocomposites. The excitation spectrum (Fig. 4a) consists of a broad band with a maximum at 254 nm and some sharp peaks in the longer wavelength region. The former is due to the charge-transfer band (CTB) of Eu^{3+}–O^{2-} bond, and the latter is due to the f–f transition lines of Eu^{3+}. Upon excitation into the CTB of Eu^{3+} at 254 nm, we obtained emission spectrum of the Y_2O_3:Eu^{3+} microspheres which contain a series of sharp lines in the region 500–700 nm (Fig. 4b). As can be seen from Fig. 4b, the emission spectrum is composed of $^5D_{0,1} \rightarrow {}^7F_J$ (J = 0, 1, 2, 3, 4) transition lines of Eu^{3+}. All the other emission peaks at 533 ($^5D_1 \rightarrow {}^7F_1$), 580 ($^5D_0 \rightarrow {}^7F_0$), 586, 592, 599 ($^5D_0 \rightarrow {}^7F_1$), 629 ($^5D_0 \rightarrow {}^7F_3$) and 706 ($^5D_0 \rightarrow {}^7F_4$) have been assigned in Fig. 4b. Under excitation at 254 nm, Y_2O_3:Eu3% microspheres emitted a strong red luminescence with a narrow peak centered at 610 nm, which can be assigned to the transition from the $^5D_0$ excited state to the $^7F_2$ state, and the spectra properties are typical for the well-known Y_2O_3:Eu^{3+} [17–23]. The decrease of the luminescence intensity of the Fe/Fe_3O_4@Y_2O_3:Eu3% nanocomposite, compared to the value of the Y_2O_3:Eu3%, can be explained by taking into account the quenching effect of the magnetic ions. The magnetic ions decrease the absorption UV energy of activator ions in host because of a strong quenching effect on the luminescence intensity. The decreased volume for the photon–solid interaction at the surface of Fe/Fe_3O_4@Y_2O_3:Eu3% nanopowder is the main reason for the decreased emission intensity.

In order to investigate the fluorescence change of the Fe/Fe_3O_4@Y_2O_3:Eu3% nanocomposites after UV light irradiation, we first discussed the fluorescence change of the pure Y_2O_3:Eu3% after UV-light irradiation. Fig. 5 is the photoluminescence excitation and emission spectra of Y_2O_3:Eu3% microspheres after UV-light irradiation for different times. Fig. 5a shows the CTB changes of Eu^{3+}–O^{2-} in Y_2O_3:Eu3% microsphere before and after UV light irradiation with the same wavelengths for different times. As can be seen from Fig. 5a, the intensities of the CTB increase with increasing the UV light irradiation time. This demonstrates that the spectra change induced by the UV irradiation is time selective. The present results are similar to that in Y_2O_3:Eu^{3+} NPS [24,25]. Under UV light irradiation, the light-induced spectra change in Y_2O_3:Eu^{3+} microspheres can be attributed to that the local environments change the surrounding of Eu^{3+} ions, instead of the photoreduction from Eu^{3+} to Eu^{2+} [24,25]. The variation of CTB with UV light is related to surface effects of the samples. The local environments for the Eu^{3+} ions in the surface are easily rearranged by UV irradiation, because of the existence of numerous surface defects, leading to a change in the CTB [25]. The disordered Eu^{3+} ions which located at local environments surface become relatively ordered. The sur-

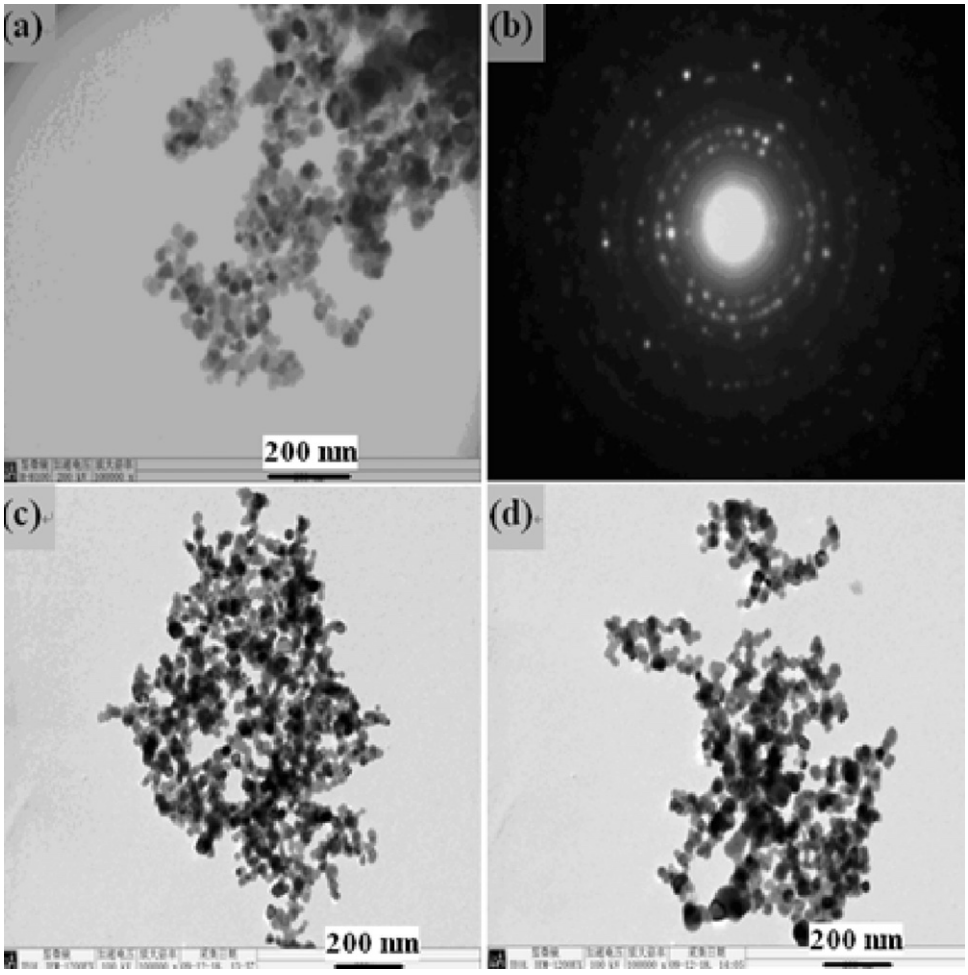

Fig. 3. TEM images of Fe_3O_4 and its SAED pattern (a) and (b), as well as TEM images of Fe_3O_4@Y_2O_3:Eu3% nanocomposites (c) and (d).

face defects such as oxygen vacancies are modified as well, leading to the enhancement of photoluminescence [26]. To further prove the reproducibility of experimental results, the samples such as YVO_4:Eu, YPO_4:Eu, YBO_3:Eu and other luminescent materials were also irradiated by UV light, the results are consistent with the results of Y_2O_3:Eu3%. Fig. 6 is the photoluminescence excitation and emission spectra of YVO_4:Eu3% after UV-light irradiation for different time.

In order to investigate the fluorescence change of the Fe/Fe_3O_4@Y_2O_3:Eu3% nanocomposites under magnetic field effects, we also discussed the fluorescence change of the pure Y_2O_3:Eu3% microspheres under magnetic field effects. Fig. 7 is the photoluminescence excitation and emission spectra of Y_2O_3:Eu3% under UV-light irradiation and magnetic field effects. As can be seen from Fig. 7a, the absorption peaks of Eu^{3+}–O^{2-} CTB transition clearly enhances under the effects of UV irradiation and the

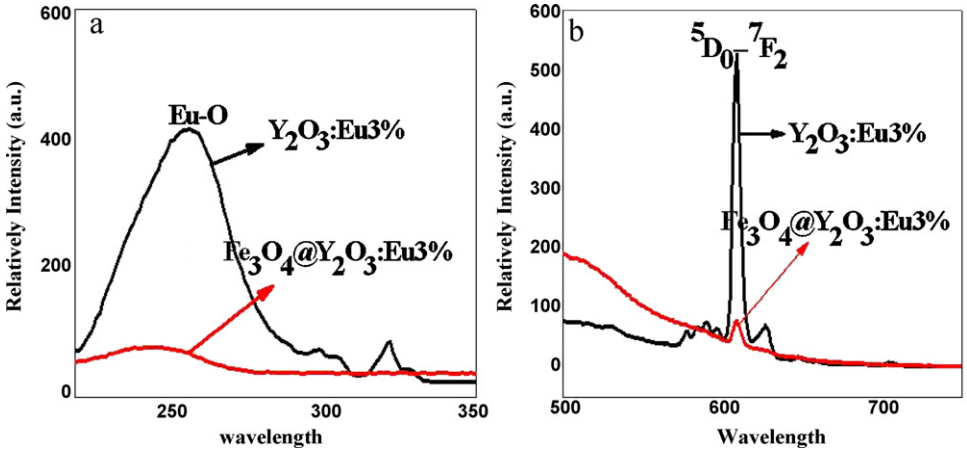

Fig. 4. Photoluminescence (a) excitation and (b) emission spectra of Y_2O_3:Eu3% microspheres and multifunctional Fe_3O_4@Y_2O_3:Eu3% nanocomposites.

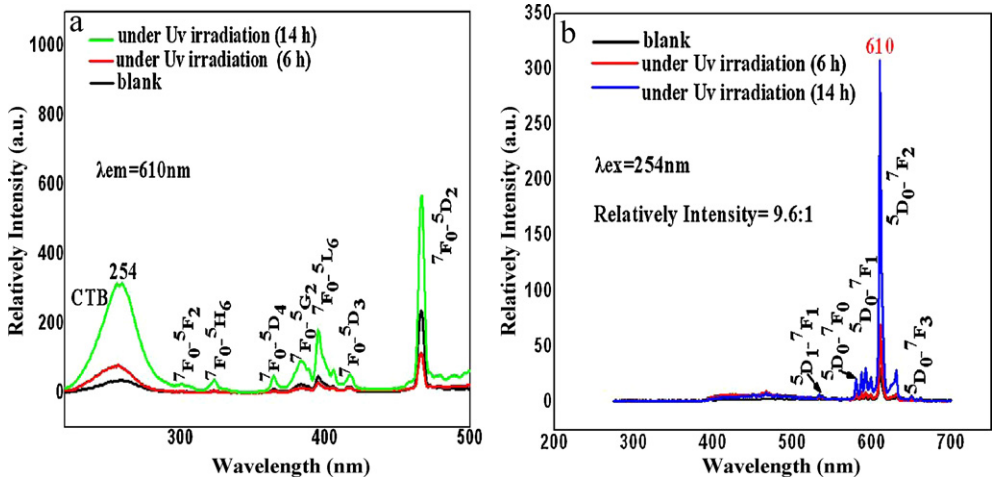

Fig. 5. Photoluminescence (a) excitation and (b) emission spectra of Y_2O_3:Eu3% microspheres after UV light irradiation for different time.

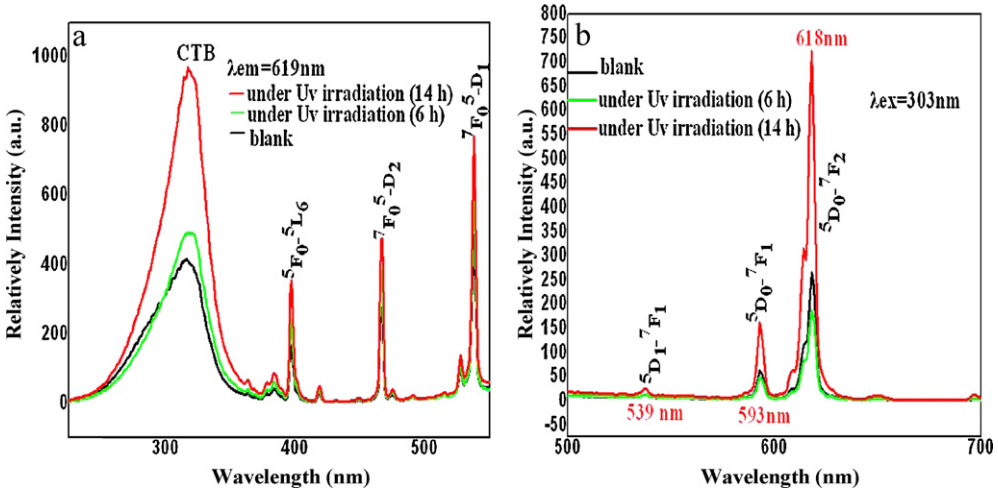

Fig. 6. Photoluminescence (a) excitation and (b) emission spectra of YVO_4:Eu3% after UV-light irradiation for different time.

magnetic field. This is mainly due to that there are many surface defects on Y_2O_3:Eu surface and the local environments for the Eu^{3+} ions in/near the surface are easily rearranged under the UV irradiation and the magnetic field effects. For example, the rearrangement of Eu^{3+} may be more inclined to order under the magnetic field effects, so the absorption peaks of Eu^{3+}–O^{2-} CTB transition influenced by magnetic field effects are stronger than the samples under UV irradiation. Fig. 7b reveals that the lumines-

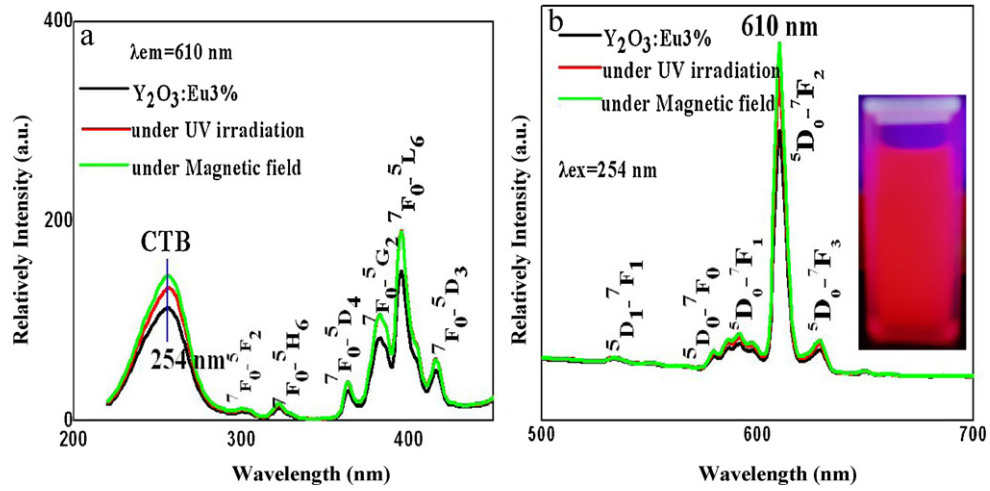

Fig. 7. Photoluminescence (a) excitation and (b) emission spectra of Y_2O_3:Eu3% under UV-light irradiation and magnetic field effects.

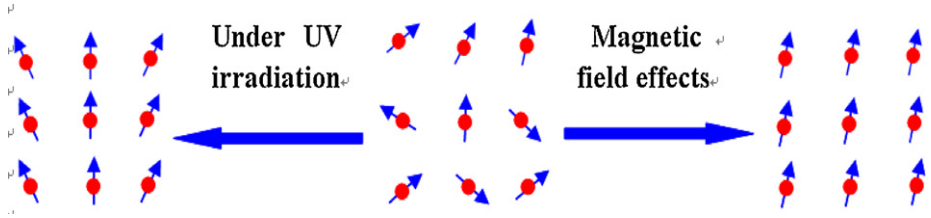

Fig. 8. The possible directed rearrangement of d–f electrons in Eu^{3+} ion.

cence intensity under magnetic field effects is also stronger than that after UV irradiation. This may be due to the fact that the d–f electrons in Eu^{3+} ions have been rearranged according to certain rules (Fig. 8). The absorption energy of the electronic transition under the magnetic field effects is larger than that after the UV irradiation. Therefore, the luminescence intensity under magnetic field effects is stronger than the sample after the UV irradiation. The possible directed rearrangement of d–f electrons in Eu^{3+} ion are shown in Fig. 8.

Fig. 9 is photoluminescence emission spectra of $Fe/Fe_3O_4@Y_2O_3$:Eu3% nanocomposites obtained under different conditions. As can be seen from Fig. 9, after the UV irradiation and the magnetic field effects, the luminescence intensity of the magnetic-fluorescent nanocomposites significantly enhanced. And the luminescence intensity of sample irradiated by UV light is stronger than that which influenced by the magnetic field effects. Interestingly, this result is just the opposite of the pure Y_2O_3:Eu3%. From the discussion of Fig. 7, we know why the luminescence intensity of Y_2O_3:Eu3% will increase after the UV irradiation and the magnetic field effects. However, the luminescence intensity of samples after UV irradiation is stronger than the effect of magnetic field (Fig. 9). This may be due to the fact that the magnetic properties of the sample which decided by the arrangement ordering of magnetic domains are decreased after the UV light irradiation. Therefore, the lower magnetic properties weaken the quenching effects on the luminescence intensity of Y_2O_3:Eu. In addition, the d–f electrons in Eu^{3+} ions will be rearranged in the transition process under the UV light irradiation. As the result, the effects of electronic cross-relaxation are weakened. And the luminescence intensity of magnetic-fluorescent nanocomposites becomes increasing.

The magnetic properties of the multifunctional nanocomposites were characterized using a superconducting quantum interference device (SQUID) magnetometer with fields up to 1 T. Fig. 10 shows the saturation magnetization curves of the as-prepared nanocomposites. Hysteresis loops of the samples were registered at room temperature (300 K). The saturation magnetization (Ms) value of Fe/Fe_3O_4 is 80 emu/g. After the $Y_2O_3:Eu^{3+}$ coating, the saturation magnetization value dropped to 2.4 emu/g. The decrease of the saturation magnetization, compared to the value of the Fe/Fe_3O_4, can be explained by taking into account the diamagnetic contribution of the thick $Y_2O_3:Eu^{3+}$ layer surrounding the Fe/Fe_3O_4 [3]. Another possible reason is that Fe_3O_4 could be oxidized to γ-Fe_2O_3 during the synthesis [27]. Generally, spin disorder on the surface and surface oxidation of nanocomposites would significantly reduce the total magnetic moment. Similar results have been observed in previous work [28,29] where the saturation magnetic value of Fe_3O_4 is reduced after coating with a shell.

After UV light irradiation, the saturation magnetization value of $Fe/Fe_3O_4@Y_2O_3:Eu^{3+}$ dropped to 2.1 emu/g. The decrease of the saturation magnetization after the UV light irradiation can be explained by the arrangement of the magnetic domains. From the view point of the microscopic atomic structure, the interaction caused by electrons spin which lead to the formation of some small spontaneous magnetization regions (magnetic domains) is very strong. In a magnetic domain, the spin magnetic moment of electrons arranged very neatly (Fig. 11), which exhibits strong magnetic properties. When the magnetic materials were irradiated by UV light, the magnetic domain which arranged very neatly became relatively disordered. That is to say the arrangements of the magnetic domains in magnet were disrupted. Therefore, the saturation

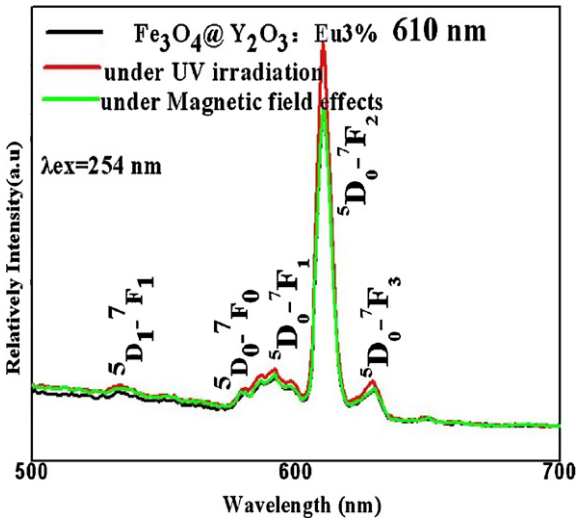

Fig. 9. Photoluminescence emission spectra of (a) $Fe_3O_4@Y_2O_3$:Eu3% nanocomposites, (b) the nanocomposite after UV-light irradiation and (c) under magnetic field effects.

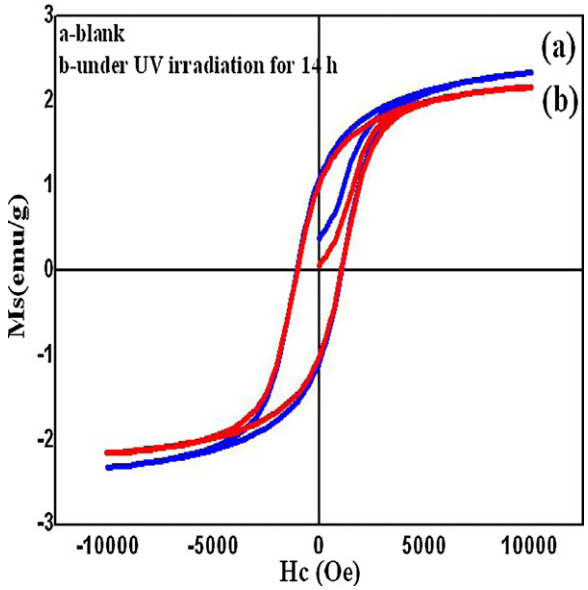

Fig. 10. Field-dependent magnetization curves of $Fe_3O_4@Y_2O_3$:Eu3% obtained under different conditions.

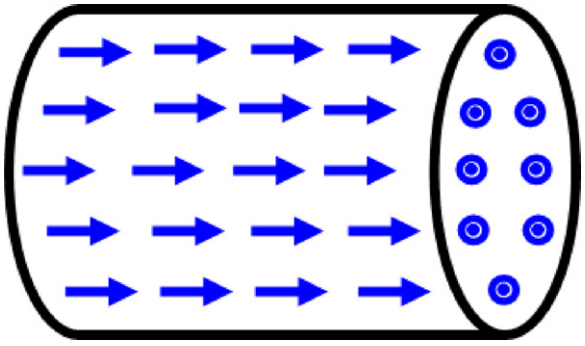

Fig. 11. The possible spontaneous magnetization regions caused by electron spins.

magnetization of the $Fe/Fe_3O_4@Y_2O_3:Eu^{3+}$ after UV light irradiation is decreased.

4. Conclusion

Multifunctional nanocomposites with Fe/Fe_3O_4 nanoparticles as the core and europium-doped yttrium oxide (Y_2O_3:Eu) as the shell ($Fe/Fe_3O_4@Y_2O_3$:Eu) have been obtained successfully employing a solvothermal method. The nanocomposites showed both ferrimagnetic behavior and unique europium fluorescence properties with high emission intensity. The spectra changes induced by the UV light irradiation and the magnetic field have been systematically studied and compared in detail. And the hysteresis curve changes induced by the UV light irradiation have been discussed. The nanocomposites could be used in a number of biomedical applications, such as drug targeting, cell separation and bioimaging.

Acknowledgement

This work is supported by National Natural Science Foundation of China.

References

[1] Z.Y. Ma, D. Dosev, M. Nichkova, S.J. Gee, B.D. Hammock, Kennedy S I.M., J. Mater. Chem. 19 (2009) 4695–4700.
[2] D. Dosev, M. Nichkova, R.K. Dumas, S.J. Gee, B.D. Hammock, K. Liu, I.M. Kennedy, Nanotechnology 18 (2007) 055102.
[3] X. Yu, J. Wan, Y. Shan, K. Chen, X. Han, Chem. Mater. 21 (2009) 4892–4898.
[4] A.K. Pradhan, R. Bah, R.B. Konda, R. Mundle, H. Mustafa, O. Bamiduro, R.R. Rakhimov, J. Appl. Phys. 103 (2008), 07F704.
[5] P. Yang, Z. Quan, Z. Hou, C. Li, X. Kang, Z. Cheng, J. Lin, Biomaterials 30 (2009) 4786–4795.
[6] T.J. Yoon, K.N. Yu, E. Kim, J.S. Kim, B.G. Kim, S.H. Yun, B.H. Sohn, M.H. Cho, J.K. Lee, S.B. Park, Small 2 (2006) 209–215.
[7] Y. Lu, Y.D. Yin, B.T. Mayers, Y.N. Xia, Nano Lett. 2 (2002) 183–186.
[8] C. Becker, M. Hodenius, G. Blendinger, A. Sechi, T. Hieronymus, D. Muller-Schulte, T. Schmitz-Rode, M. Zenke, J. Magn. Magn. Mater. 311 (2007) 234–237.
[9] X. Hong, J. Li, M.J. Wang, J.J. Xu, W. Guo, J.H. Li, Y.B. Bai, T.J. Li, Chem. Mater. 16 (2004) 4022–4027.
[10] Y.M. Huh, Y.W. Jun, H.T. Song, S. Kim, J.S. Choi, J.H. Lee, S. Yoon, K.S. Kim, J.S. Shin, J.S. Suh, J. Cheon, J. Am. Chem. Soc. 127 (2005) 12387–12391.
[11] G.H. Du, Z.L. Liu, Q.H. Lu, X. Xia, L.H. Jia, K.L. Yao, Q. Chu, S.M. Zhang, Nanotechnology 17 (2006) 2850–2854.
[12] F. Bertorelle, C. Wilhelm, J. Roger, F. Gazeau, C. Menager, V. Cabuil, Langmuir 22 (2006) 5385–5391.
[13] C.F. Tu, Y.H. Yang, M.Y. Gao, Nanotechnology 19 (2008) 8.
[14] J.H. Gao, B. Zhang, Y. Gao, Y. Pan, X.X. Zhang, B. Xu, J. Am. Chem. Soc. 129 (2007) 11928–11935.
[15] H.W. Gu, R.K. Zheng, X.X. Zhang, B. Xu, J. Am. Chem. Soc. 126 (2004) 5664–5665.
[16] H.C. Lu, G.S. Yi, S.Y. Zhao, D.P. Chen, L.H. Guo, J. Cheng, J. Mater. Chem. 14 (2004) 1336–1341.
[17] J. Yang, Z. Quan, D. Kong, X. Liu, J. Lin, Cryst. Growth Des. 4 (2007) 731.
[18] M.K. Devaraju, S. Yin, T. Sato, Nanotechnology 20 (2009) 305302.
[19] Y. Bai, Y. Wang, G. Peng, W. Zhang, Y. Wang, K. Yang, X. Zhang, Y. Song, Opt. Commun. 282 (2009) 1922.
[20] Q. Li, L. Gao, D. Yan, Chem. Mater. 11 (1999) 533–535.
[21] C.A. Traina, J. Schwartz, Langmuir 23 (2007) 9158–9161.
[22] X. Li, Q. Li, Z. Xia, L. Wang, W. Yan, J. Wang, R.I. Boughton, Cryst. Growth Des. 6 (2006) 2193.
[23] G.K. Das, T.T.Y. Tan, J. Phys. Chem. C 112 (2008) 11211–11217.
[24] X. Bai, H. Song, L. Yu, L. Yang, Z. Liu, G. Pan, S. Lu, X. Ren, Y. Lei, L. Fan, J. Phys. Chem. B 109 (2005) 15236–15242.
[25] H. Song., B. Chen, P.H. Zhang, J. Appl. Phys. Lett. 81 (2002) 1776.
[26] J. Wang, H. Song, B. Sun, X. Ren, B. Chen, W. Xu, Chem. Phys. Lett. 379 (2003) 507.
[27] E. Tronc, P. Belleville, J.J.P. Livage, J. Langmuir 8 (1992) 313.
[28] H.H. Lu, G.H. Yi, S.Y. Zhao, D.P. Chen, L.H. Guo, J. Cheng, J. Mater. Chem. 14 (2004) 1336.
[29] L.Y. Wang, J. Luo, Q. Fan, M. Suzuki, I.S. Suzuki, M.H. Engelhard, Y.H. Lin, N. Kim, J.Q. Wang, C.J. Zhong, J. Phys. Chem. B 109 (2005) 21593.